Intensification of Geostrophic Currents in the Canada Basin, Arctic Ocean

MILES G. MCPHEE

McPhee Research Company, Naches, Washington

(Manuscript received 24 May 2012, in final form 28 November 2012)

ABSTRACT

Continuous sampling of upper-ocean hydrographic data in the Canada Basin from various sources spanning from 2003 through 2011 provides an unprecedented opportunity to observe changes occurring in a major feature of the Arctic Ocean. In a 112-km-radius circle situated near the center of the traditional Beaufort Gyre, geopotential height referenced to 400 dbar increased by about 0.3 gpm from 2003 to 2011, and by the end of the period had increased by about 65% from the climatological value. Near the edges of the domain considered, the anomalies in dynamic height are much smaller, indicating steeper gradients. A rough dynamic topography constructed from profiles collected between 2008 and 2011 shows the center of the gyre to have shifted south by about 2° in latitude, along the 150°W meridian. Geostrophic currents are much stronger on the periphery of the gyre, reaching amplitudes 5–6 times higher than climatological values at grid points just offshore from the Beaufort and Chukchi shelf slopes. Estimates of residual buoy drift velocity after removing the expected wind-driven component are consistent with surface geostrophic currents calculated from hydrographic data. A three-decade time series of integrated ocean surface stress curl during late summer near the center of the Beaufort Gyre shows a large increase in downward Ekman pumping on decadal scales, emphasizing the importance of atmospheric forcing in the recent accumulation of freshwater in the Canada Basin. Geostrophic current intensification appears to have played a significant role in the recent disappearance of old ice in the Canada Basin.

1. Background

The Beaufort Gyre (BG) in the Canada Basin of the Arctic Ocean is both a major repository of marine freshwater for the World Ocean (Aagaard and Carmack 1989; Carmack et al. 2008; Proshutinsky et al. 2009) and, until recently, the primary refuge for thick, multiyear pack ice in the Arctic (Rigor and Wallace 2004; Nghiem et al. 2007; Maslanik et al. 2011). McPhee et al. (2009) compared data from an airborne hydrographic survey in late winter of 2008 with the Polar Hydrographic Climatology ocean database version 3.0 (PHC 3.0) compiled by Steele et al. (2001), to estimate that liquid freshwater content (FWC) had increased by 26% in the Canada and Makarov Basins, while decreasing by 26% in the Eurasian Basin for a net increase of about 7700 km^3, similar to results based on summer data reported by Rabe et al. (2011).

Closely connected to changes in FWC are changes in dynamic topography. If FWC increase is not uniformly distributed, the pressure gradient associated with sea surface elevation will change. In a west-to-east section bisecting the traditional (climatological) Beaufort Gyre during the 2008 survey, McPhee et al. (2009) reported a significant modification of surface geostrophic currents, with a large increase in northward freshwater transport. More recently, Kwok and Morison (2011) combined hydrographic and satellite altimeter data to construct a dynamic topography for the entire Arctic Basin reflecting conditions during the first part of the present century, confirming increased freshwater content in the Canada Basin and more saline upper-ocean conditions in the Eurasian Basin.

Increased liquid freshwater and associated spinup of the Beaufort Gyre have been associated with anticyclonic atmospheric pressure (Proshutinsky et al. 2002, 2009). Ogi et al. (2008) suggested that anticyclonic winds during the summer of 2007 contributed to the unprecedented sea ice retreat observed that year. Ogi and Wallace (2012) extended the analysis to subsequent years, concluding that ''from 2007 onward, the low level circulation over the Arctic has been much more anticyclonic than in prior years....'' They explicitly refuse to

Corresponding author address: Miles G. McPhee, McPhee Research Company, 450 Clover Springs Road, Naches, WA 98937.
E-mail: mmcphee@hughes.net

DOI: 10.1175/JCLI-D-12-00289.1

speculate as to the origin of the recent anticyclonic wind anomalies. On the other hand, Morison et al. (2012) argue that a cyclonic shift in the transport of Eurasian runoff associated with high winter Arctic Oscillation indices (anomalously low pressure) from 2005–08 accounts for the increase in FWC of the Canada Basin, rather than the strength of the wind-driven Beaufort Gyre.

Beginning in 2003, the Beaufort Gyre Exploration Program (BGEP; http://www.whoi.edu/beaufortgyre) has annually seeded the Canada Basin with unmanned Ice-Tethered Profiler (ITP) buoys equipped with profiling instrumentation that return data on the water column to approximately 700 m up to twice daily in near real time (http://www.whoi.edu/itp/; Krishfield et al. 2008). Since 2003, ITP data, combined with extensive shipboard surveys performed during the late summer BGEP cruises, and including data from the 2008 International Polar Year (IPY) survey [North Pole Environmental Observatory (NPEO); http://psc.apl.washington.edu/northpole], have provided unprecedented coverage of this previously poorly sampled region, in all seasons.

Based on the recent hydrographic data, this paper reports an analysis of dynamic circulation changes in the Canada Basin, with emphasis on the period following the 2008 IPY survey. It finds that freshwater continues to accumulate in the Beaufort Gyre, resulting in a surprising increase in the surface geostrophic currents on the periphery of the gyre. This appears to be directly related to the observed anomaly in summer anticyclonic winds, and it is speculated that this in turn results from much larger temperature contrasts across the Canada Basin associated with open water in the western part of the basin where surface geostrophic currents are northward. The increased circulation strength also seems to have played a critical role in the recent disappearance of old ice in the Canada Basin.

2. Methods and results

Density in cold seawater is dominated by salinity, so at high latitudes there is strong connection between FWC and geopotential height (Z) of the ocean surface. By convention, Z is expressed in terms of geopotential anomaly divided by gravity, $Z = -\Phi'(p)/g$ (e.g., Gill 1982), with units of geopotential meters (gpm). If geostrophic flow at some pressure level, p_{ref}, is small, then geostrophic velocity at the surface ($\mathbf{v}_g$ when $p = 0$) is

$$f\mathbf{k} \times \mathbf{v}_g \approx -\nabla\Phi'(p_{\mathrm{ref}}), \tag{1}$$

where f is the Coriolis parameter. Here Z is calculated from geopotential anomaly at $p_{\mathrm{ref}} = 4 \times 10^6$ Pa (400 dbar), so that geostrophic surface velocity is relative to a level of about 400 m. Compared with climatology, recent freshening has been largely confined to the upper 400 m, and tests with different reference pressures confirmed that below 400 dbar the relative geopotential anomaly gradients were small.

Data were assembled for the Canada Basin from the sources cited above. ITP data were culled by considering only profiles that covered the water column from 8-m to at least 500-m depth, and for which there was little deviation in salinity at 400 m from the overall average. All IPY 2008 aerial survey data for the Canada Basin were included [except air-dropped expendable conductivity–temperature–depth (CTD) probes], as were available BGEP shipboard measurements from 2003 through 2010 (418 stations). Combined, these provided 8853 acceptable profiles for the period from 2003 through 2011.

For the period from 2004 to early (winter) 2008, Kwok and Morison (2011) reported a doming of about 40+ cm relative to the geoid in the Beaufort Gyre, based on a dynamic ocean topography (DOT) for the Arctic computed from winter *ICESat* altimeter data. Here we consider a surface geopotential height topography relative to the 400-dbar pressure constructed from available hydrography observations during the most recent calendar years, 2008–11 (Fig. 1a). The geopotential anomaly at the 400-dbar pressure surface was computed for each profile, with results fitted via Delaunay triangulation to a polarstereographic coordinate grid with 50-km grid spacing. Arrows indicate surface geostrophic currents calculated from (1). Spatial coverage (gray dots) is more complete in the northeast, reflecting the necessity of finding suitable ice for ITP deployments in late summer. Note the peak in Z centered at around 74.5°N, 150°W.

For comparison, the calculation was repeated using the PHC 3.0 climatology, interpolated to the profile positions, fitted to the same grid, and then plotted with the same scale shading in Fig. 1b. Note, however, that the velocity scale differs from Fig. 1a by a factor of 4, and that on the periphery of the BG, geostrophic current magnitudes are now as much as 5–6 times larger than the climatological values. Time series discussed below pertain to the region enclosed by the dashed circle in Fig. 1b, with a radius of 112 km centered at 75°N, 150°W, about midway between the recent and climatological BG centers.

The trajectory of ITP55 nearly bisected the recent BG position (Fig. 1a) in an east-to-west direction (Fig. 2a). The buoy, deployed in early August 2011, began its westward sweep across the deep Canada Basin on about 20 September 2011. As indicated at the westernmost

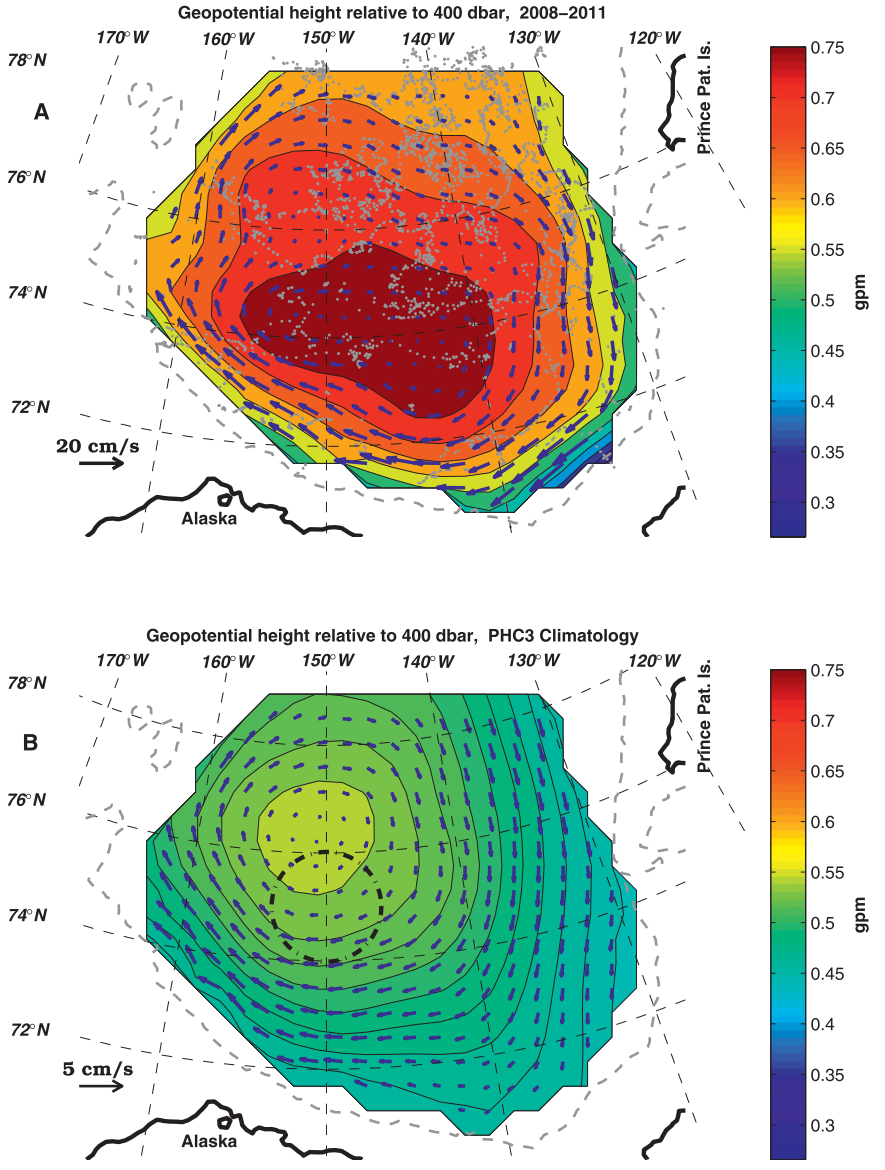

FIG. 1. (a) Contours of Z from all stations for 2008–11 interpolated to a 50 km × 50 km grid. Arrows indicate surface geostrophic current, calculated from the numerical gradient of geopotential anomaly at 400 dbar. Gray dots show station locations. The solid black curve shows the coastline; the dashed curve is the 400-m isobath. (b) As in (a), but calculated from PHC 3.0 climatology, interpolated to each station location. The dashed circle centered at 75°N, 150°W (112-km-radius circle) indicates the region considered for time series in Figs. 4 and 5.

stations, it encountered shallow water (<700-m depth), and "ran aground," providing its last complete profile on 11 December 2011. Surface geopotential heights (Fig. 2b) were projected onto a straight line fitted through the drift positions (dashed line in Fig. 2a), along with climatological values evaluated at the same locations. At its maximum, approximately 300 km from the Chukchi slope, Z is about two-thirds greater than its climatological counterpart. Components of geostrophic surface velocity perpendicular to the line, determined from slopes of the fitted functions (Fig. 2b), are shown as arrows in Fig. 2a. This particular instantiation from one buoy drift in late 2011 confirms the large increase in geostrophic currents offshore from the Chukchi shelf indicated by dynamic topography (Fig. 1a).

A different view of the impact of baroclinic currents is provided by comparing the actual drift of ITP 55 with its expected "free-drift" displacement calculated from

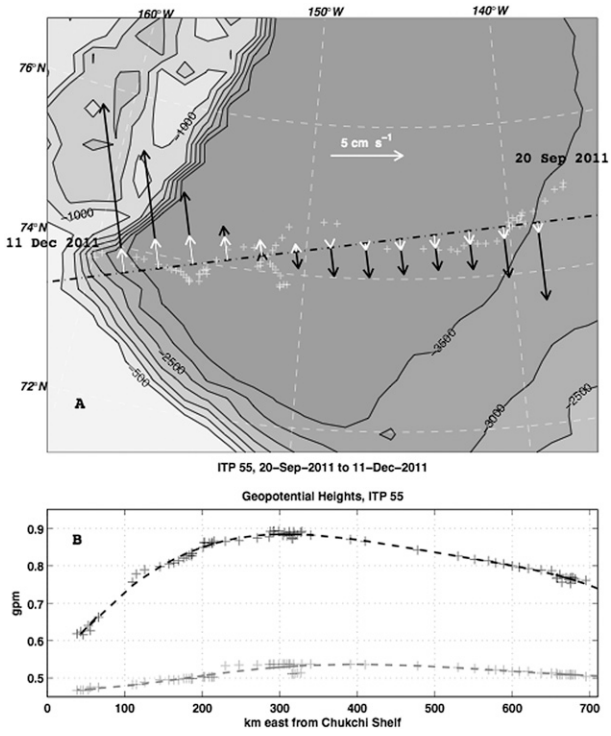

FIG. 2. (a) ITP 55 profile locations as it drifted across the Beaufort Gyre, 20 Sep–11 Dec 2011 (plus symbols), superimposed on bathymetry. Vectors indicate geostrophic surface current perpendicular to a linear fit to the positions (dot-dashed line) for 2011 observations (black) and PHC 3.0 climatology at same locations (white). (b) Dynamic heights for each profile (black plus symbols), projected onto the trajectory line and then fitted with a fifth-order polynomial (dashed curve). Gray symbols and curve are similar calculations for the climatological data.

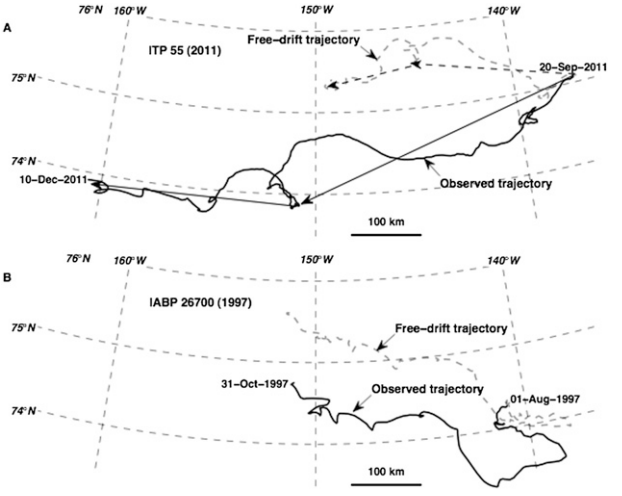

FIG. 3. (a) Comparison of ITP 55 trajectory across the BG in 2011 (black) along with the "free-drift" trajectory (dashed) inferred from 10-m NCEP CFSR wind interpolated to the actual buoy locations. Solid and dashed arrows indicate total displacements before and after the SE excursion on 3 November in the observed and free-drift trajectories, respectively. (b) As in (a), but for IAPB buoy 26700 for 1 Aug–31 Oct 1997.

surface wind (Fig. 3a). Neglecting internal ice stress gradients, the free-drift force balance

$$imf\hat{V}_{\rm wd} = \rho_a c_{10} W_{10} \hat{W}_{10} - \rho_w u_{*0} \hat{u}_{*0} \qquad (2)$$

was solved at 6-h intervals, forced by the National Centers for Environmental Prediction (NCEP) Climate Forecast System Reanalysis (CFSR) 10-m wind field (Saha et al. 2010), interpolated to the actual buoy positions. Here $\hat{V}_{\rm wd}$ is the complex wind-driven component of ice velocity; m is the ice mass per unit area; ρ_a and ρ_w are air and water density, respectively; and $\hat{u}_{*0}$ is friction velocity at the ice–water interface, related to $\hat{V}_{\rm wd}$ by a Rossby-similarity drag relation (McPhee 2008, 2012):

$$\frac{\hat{V}_{\rm wd}}{\hat{u}_{*0}} = \frac{1}{\kappa}\left(\log\frac{u_{*0}}{fz_0} - A - iB\right). \qquad (3)$$

Since friction velocity depends on $\hat{V}_{\rm wd}$, (2) and (3) are solved iteratively from an initial guess, with parameters appropriate for the Surface Heat Budget of the Arctic Ocean (SHEBA) drift (Persson et al. 2002; McPhee 2008) and ice draft equal to 2 m. The integrated wind-driven component accounts for less than half of the total displacement (342 vs 703 km). The brief southeastward excursion in early November 2011 conveniently divides the drift into two segments, as indicated by the arrows in Fig. 3a. During the first period, when the buoy is east of 150°W, there is a strong southwest component of drift not accounted for by the wind. In the latter period, the west-northwest residual drift is again considerably larger than the wind-driven component.

A similar calculation (Fig. 3b) compares the actual drift of an International Arctic Buoy Program (IABP; http://iabp.apl.washington.edu/) buoy in 1997 with its integrated free-drift trajectory, again based on NCEP CFSR winds, and otherwise forced with identical parameters. On 1 August 1997, IABP 26700 was about 120 km southwest of the position of ITP 55 on 20 September 2011, and over the next three months drifted about 300 km westward. The wind-driven drift is similar for both buoys, indicating similar average winds. The obvious difference is that in 1997 the magnitudes of the observed and wind-driven components were similar, with most of the residual drift due to geostrophic current occurring early on when the buoy was toward the eastern edge of the BG. As discussed below, average ice thickness over the BG has decreased substantially since 1997; however, ITP 55 was deployed in relatively thick

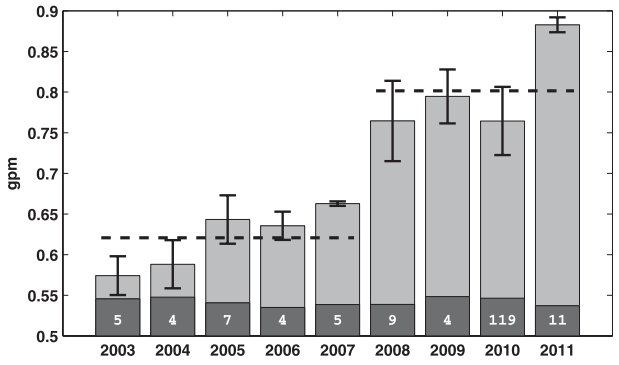

FIG. 4. Annual average Z values observed from 2003 through 2011 (light gray shading) for all profiles within a 1° radius circle centered at 75°N, 150°W. Numerals list the number of profiles in each year. Error bars mark ± one standard deviation of the observations. Also shown are averages of PHC3.0 climatological data evaluated at the profile locations (darker shading). Dashed lines are overall average values prior to, and after, 2008.

ice (3.13 m), so assuming similar ice characteristics for regions surrounding the two buoys is probably reasonable.

Since the BG ''dome'' in recent years is considerably higher than the PHC 3.0 climatology or the 2004–08 DOT computed by Kwok and Morison (2011) [see also similar results reported by Farrell et al. (2012)], we examined temporal changes in a region near the BG center (Fig. 4). Within the 112-km circle centered at 75°N, 150°W, for the 9 yr in which ITP data have been available, there has been a striking increase in Z from within a few geopotential centimeters of climatology in 2003 to nearly 65% greater by 2011. The increased dome elevation combined with a southward shift of its position and lack of corresponding increase in FWC near the continental shelf north of Alaska accounts for the dramatic increase in geostrophic currents offshore of the Beaufort and Chukchi shelves.

3. Discussion

The present analysis suggests that geostrophic current magnitudes in the BG are now often comparable to ice drift speeds typically associated with moderately intense wind events. This appears to be driven by persistent convergence of freshwater by Ekman transport in the ice/ocean and open ocean boundary layers, especially during summer. Morison et al. (2012) argue that since the period from 2005 to 2008 was characterized by relatively increased cyclonic atmospheric conditions over the wintertime Arctic (higher Arctic Oscillation index), increase of freshwater (FW) in the Canada Basin resulted more from transport of Eurasian river runoff from the Siberian shelves across the northern reaches of the gyre than from Ekman convergence in the surface boundary layer. The more localized approach taken here differs by suggesting that in summer seasonally available freshenings from melting and runoff, along with strongly stratified near-surface conditions, combine to herd FW toward the BG center under relatively strong anticyclonic summer atmospheric conditions.

Ogi et al. (2008) and Ogi and Wallace (2012) demonstrated that low September ice extent is associated with anomalous, late summer anticyclonic sea level pressure over the Arctic, which has been persistent over the past decade. They argued that herding by Ekman drift away from the periphery toward the central Arctic played an important role in the record low ice extent of 2007. Ekman drift of sea ice is closely related to cross-isobar transport of water in the ice–ocean boundary layer (IOBL). Averaged over inertial cycles, volume transport in the IOBL is ideally directed 90° clockwise in the Northern Hemisphere (NH) from kinematic stress at the ocean surface, equal to its magnitude divided by the Coriolis parameter. Divergence of volume transport is thus proportional to the curl of navifacial stress, and by continuity, the difference between vertical velocity (Ekman pumping) at the base of the boundary layer and the surface is

$$w_p \approx \frac{1}{f}\nabla \times \hat{\boldsymbol{\tau}}_0, \tag{4}$$

where $\hat{\boldsymbol{\tau}}_0$ is the horizontal kinematic stress at the ocean boundary. Compact, thick ice can substantially modify the transfer of wind stress to the ocean; however, in late summer [August–October (ASO)], internal ice forces are often small relative to wind stress (McPhee 1980, 2008), and the force balance is approximately

$$\hat{\boldsymbol{\tau}}_0 \approx \hat{\boldsymbol{\tau}}_a - if d_{\text{ice}} \hat{V}_{\text{wd}}, \tag{5}$$

where $\hat{\boldsymbol{\tau}}_a$ is wind stress divided by water density, d_{ice} is ice draft, and $\hat{V}_{\text{wd}}$ is the wind-driven component of ice velocity, estimated as above. Daily values of NCEP CFSR wind stress, ice thickness, and ice concentration fields were used to calculate w_p fields from (4) and (5), for the ASO time periods in each year from 1980 through 2011, which were then integrated over time to get net Ekman pumping displacements (a measure of total ocean boundary layer divergence) at grid points within the 112-km-radius circle centered at 75°N, 150°W (Fig. 5). While there is large interannual variability, a downward trend over the 30-yr period is apparent, with mean downward Ekman pumping in the most recent decade increasing almost fourfold from the 1982–91 decade.

A comparison of average ASO displacements from the first and last decades of the NCEP CFSR record over

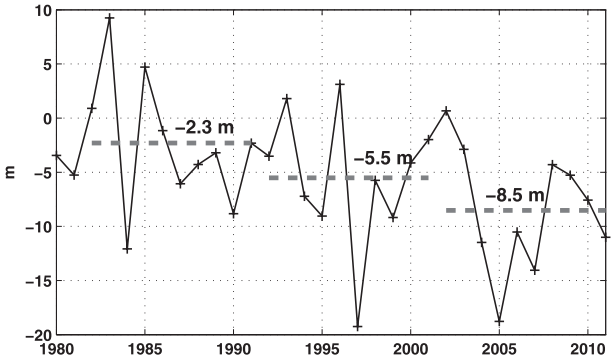

FIG. 5. Three-month integral of daily Ekman pumping velocity for the period August–October in each year, averaged over the BG ''dome'' circle centered at 75°N, 150°W. Dashed lines show decadal averages starting in 1982. (NCEP CFSR data; Saha et al. 2010).

the larger BG region (Figs. 6a,b) reveals a major expansion and northward shift in late summer downwelling, with much of the area north of 76°N having switched signs. Even under relatively compact sea ice, the IOBL warms during summer, and some of this heat becomes trapped below the shallower, seasonal mixed layer that forms as ice melt accumulates (e.g., Maykut and McPhee 1995; Jackson et al. 2010). By comparing profiles from ITP buoys that drifted near one location (79.2°N, 138.5°W) at different times from September 2007 to May 2008, McPhee et al. (2009, their Fig. 3) showed downwelling of the 2007 summer thermal signature of roughly 30 m by the following spring. Applying the stress curl calculation described above at that location over the same time span resulted in a downward displacement of about 35 m. Instead of being mixed back to the surface during freeze-up, some of the summer heating absorbed in the upper ocean is transported downward by Ekman pumping (Jackson et al. 2010; Yang 2009), and the relatively close correspondence between calculated and observed Ekman pumping in 2007–08 suggests that, at least in recent years with relatively weak ice, the pack often transmits stress to the ocean efficiently, even in winter. Figure 6b also indicates that in the northern part of the gyre, where in previous decades upwelling probably enhanced upward heat flux, now the IOBL apparently contributes heat to the lower layers.

In the first decade of the NCEP CFSR record, the BG remained effectively ice covered for the entire year, whereas over the immediate past decade, by late summer the concentrated pack retreats almost 600 km farther north on the western side of the BG. In the east, the retreat is less dramatic as the wind and currents transport ice southward. Because of the large disparity in albedo between compact sea ice and open water, horizontal thermal gradients are now much more intense during summer than in the past (Steele et al. 2008), conceivably providing an important late summer boost to the observed increase in stress curl.

Changes in ocean circulation may play a major role in equally dramatic changes in Arctic sea ice concentration, age, and thickness observed over the past two decades (Rigor and Wallace 2004; Nghiem et al. 2007; Maslanik et al. 2011). Average September ice extent over the entire Arctic reached a record minimum value (4.3×10^6 km^2) in 2007 [National Snow and Ice Data Center (NSIDC) data; Fetterer et al. 2007]. The following September, Arctic-wide ice extent had increased by about 10% (4.7×10^6 km^2) but, over the deep Canada Basin, in 2008 the ice was nearly 200 km north of its 2007 position (NSIDC data; Cavalieri et al. 1996, updated yearly; Meier et al. 2006, updated quarterly), consistent with northward geostrophic velocities inferred from a section across most of the Canada Basin in March 2008 (McPhee et al. 2009). Since 2007, the ice edge at minimum extent reaches far north in the western part of the Canada Basin with a distinct southward extension in the east, more or less tracing the surface geostrophic velocity distribution (Fig. 1a).

Maslanik et al. (2011) report that multiyear ice coverage in the Beaufort Gyre and Canada Basin decreased by 83% from 2002 to 2009. An associated animation of ice age in the Arctic (http://www.climatewatch.noaa.gov/article/2012/arctic-sea-ice-getting-thinner-younger) illustrates how older ice is now swept along the shelf slope north of Canada and Alaska, then north to melt or enter the transpolar drift stream (especially in 2011). Considering this along with the drift trajectories depicted in Fig. 3, it seems that more intense currents now present on the periphery of the Beaufort Gyre are instrumental in preventing old ice from crossing into and collecting in the center of the gyre, which in the previous century was a primary refuge for strong multiyear ice in the Arctic. The following thought experiment illustrates this. Starting with a region of multiyear ice, centered at 74°N, 133°W (about 200 km west of Banks Island) at the end of June (near the summer solstice), consider two simulated trajectories covering the next three months [July–September (JAS)], each comprising an integral of ice velocity estimated by combining the local wind-driven component [from (2) and (3), using NCEP–CFSR 10-m winds and SHEBA ice properties] with surface geostrophic velocities from the recent (Fig. 1a) and climatological (Fig. 1b) dynamic topographies, respectively. Results of this calculation for three recent years, 2009–11 (Fig. 7), show that in each year the hypothetical ice pack drifts much farther west under the influence of recent surface geostrophic currents than would have been expected under climatological conditions. Also shown in

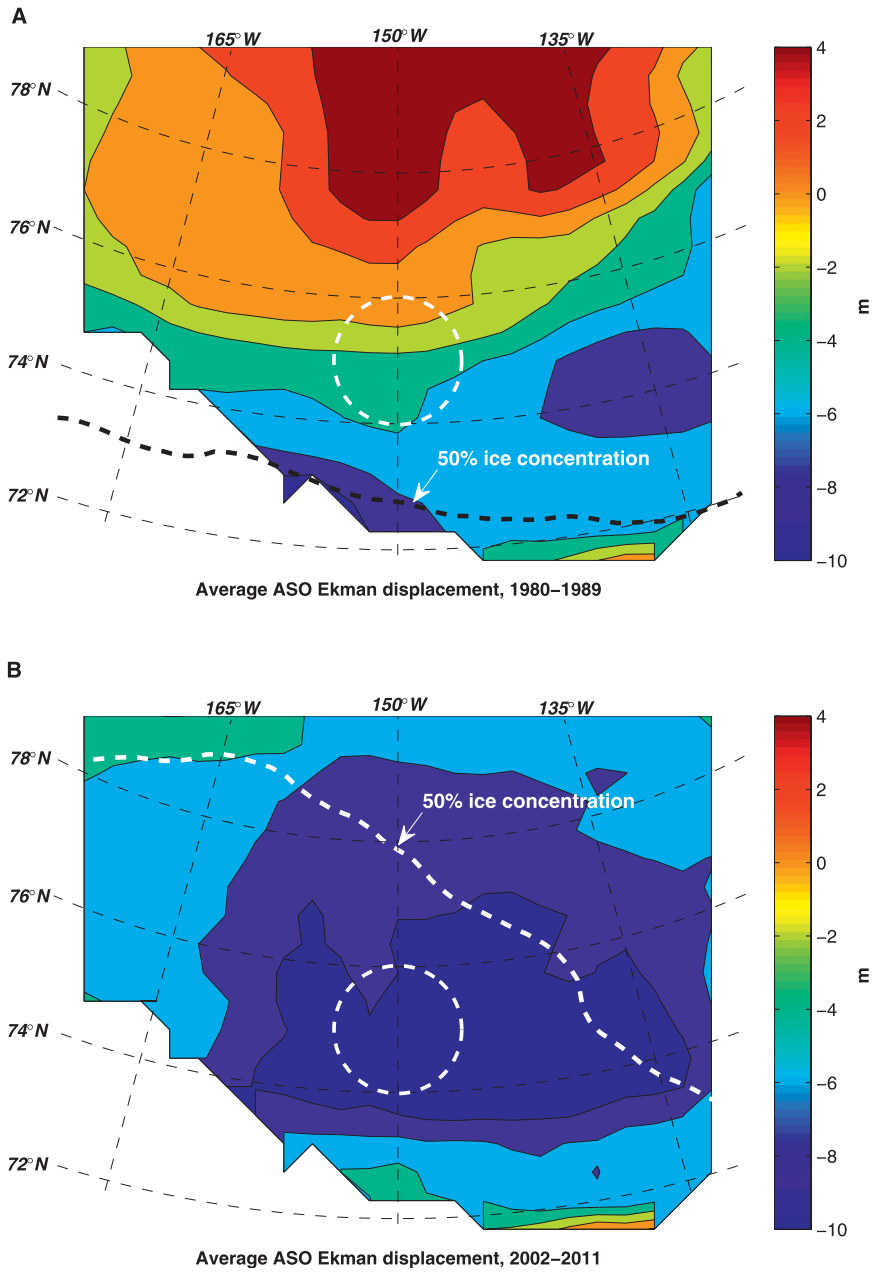

FIG. 6. (a) Ten-year average of integrated Ekman pumping for August–October of each year during the first decade of the NCEP CFSR record. The dashed circle (white) shows the area considered for the time series of Fig. 5. Also shown is the average location of September compact ice extent (50% isopleth) for the decade (Meier et al. 2006, updated quarterly). (b) As in (a), but for the most recent decade.

Fig. 7 are the mean September ice edge locations (15% concentration; Meier et al. 2006, updated quarterly), showing that the hypothetical trajectories with recent geostrophic currents all reach well into open water (and are presumed to have melted), whereas for the most part ice advected by the climatological currents in addition to wind drift would survive within the actual ice pack, certainly for ice coverage prior to 2008. Note also the close correspondence between the southward ice lobes observed in the eastern Canada Basin in recent summers and the southward geostrophic currents there. A reasonable inference from this exercise is that the present advective current structure not only reduces the tendency for multiyear ice to collect near the center of the

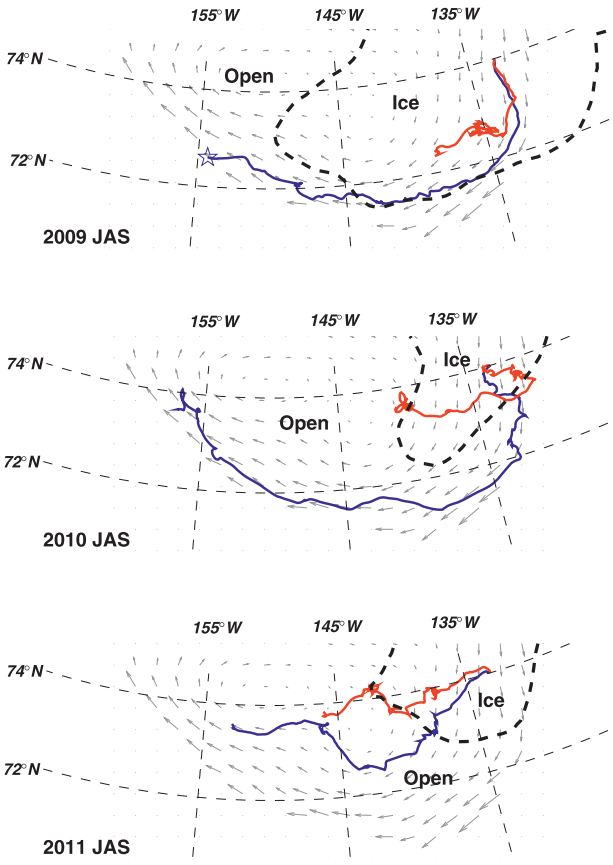

FIG. 7. Hypothetical ice displacements, July–September in 3 yr, obtained by combining wind-driven component of ice velocity with geostrophic current for 2008–11 (blue) or with geostrophic current from PHC 3.0 climatology (red). Light gray arrows correspond to $\mathbf{v}_g$ as in Fig. 1a. Dashed curves indicate the mean September ice extent (15% ice concentration isopleth; NSIDC data; Meier et al. 2006, updated quarterly). For 2009, the pentagram marks departure of the simulated trajectory from the dynamic topography domain on 20 September.

Beaufort Gyre, but also significantly enhances overall melting.

An interesting possibility is a positive feedback between the recent concentration of freshwater in the Canada Basin, with its associated geostrophic current intensification, and the atmospheric conditions that converge surface waters. Ogi et al. (2008) and Ogi and Wallace (2012) document positive anomalies in summer anticyclonic atmospheric conditions over the Canada Basin in recent years. As mentioned above, the thermal contrast between open water and sea ice may reinforce this tendency. Since albedo is mainly a function of the presence of ice, this contrast may persist as long as there is sufficient winter production in the north to keep the eastern Canada Basin ice covered for most of the summer. This scenario, considered in combination with the geopotential height time series of Fig. 4, suggests that the major circulation feature of the western Arctic Ocean, the Beaufort Gyre, is continuing to accumulate freshwater and remains in a state of rapid flux.

Acknowledgments. Motivation for this work grew from discussions with J. M. Wallace, M. Ogi, and C. Bitz, for which I am grateful. Comments from two anonymous reviewers were also helpful. Funding was provided by NSF, Office of Polar Programs, through Grants ARC0906820 and ARC0856214. The Ice-Tethered Profiler data were collected and made available by the Ice-Tethered Profiler Program (Toole et al. 2011; Krishfield et al. 2008) based at the Woods Hole Oceanographic Institution (http://www.whoi.edu/itp). Data were also collected and made available by the Beaufort Gyre Exploration Program based at the Woods Hole Oceanographic Institution (http://www.whoi.edu/beaufortgyre) in collaboration with researchers from Fisheries and Oceans Canada at the Institute of Ocean Sciences.

REFERENCES

Aagaard, K., and E. C. Carmack, 1989: The role of sea ice and other fresh water in the Arctic circulation. *J. Geophys. Res.,* **94** (C10), 14 485–14 498.

Carmack, E., F. McLaughlin, M. Yamamoto-Kawai, M. Itoh, K. Shimada, R. Krishfield, and A. Proshutinsky, 2008: Freshwater storage in the Northern Ocean and the special role of the Beaufort Gyre. *Arctic–Subarctic Ocean Fluxes: Defining the Role of the Northern Seas in Climate,* R. R. Dickson et al., Eds., Springer, 145–169.

Cavalieri, D., C. Parkinson, P. Gloersen, and H. J. Zwally, 1996: Sea ice concentrations from *Nimbus-7* SMMR and DMSP SSM/I-SSMIS passive microwave data. National Snow and Ice Data Center, Boulder, CO, digital media. [Available online at http://nsidc.org/data/docs/daac/nsidc0051_gsfc_seaice.gd.html.]

Farrell, S. L., D. C. McAdoo, S. W. Laxon, H. J. Zwally, D. Yi, A. Ridout, and K. Giles, 2012: Mean dynamic topography of the Arctic Ocean. *Geophys. Res. Lett.,* **39,** L01601, doi:10.1029/2011GL050052.

Fetterer, F., K. Knowles, W. Meier, and M. Savoie, 2007: Sea ice index. National Snow and Ice Data Center, Boulder, CO, digital media. [Available online at http://nsidc.org/data/seaice_index/.]

Gill, A. E., 1982: *Atmosphere–Ocean Dynamics.* Academic Press, 662 pp.

Jackson, J. M., E. C. Carmack, F. A. McLaughlin, S. E. Allen, and R. G. Ingram, 2010: Identification, characterization, and change of the near-surface temperature maximum in the Canada Basin, 1993–2008. *J. Geophys. Res.,* **115,** C05021, doi:10.1029/2009JC005265.

Krishfield, R., J. Toole, A. Proshutinsky, and M.-L. Timmermans, 2008: Automated ice-tethered profilers for seawater observations under pack ice in all seasons. *J. Atmos. Oceanic Technol.,* **25,** 2091–2105.

Kwok, R., and J. Morison, 2011: Dynamic topography of the ice-covered Arctic Ocean from ICESat. *Geophys. Res. Lett.,* **38,** L02501, doi:10.1029/2010GL046063.

Maslanik, J., J. Stroeve, C. Fowler, and W. Emery, 2011: Distribution and trends in Arctic sea ice age through spring 2011. *Geophys. Res. Lett.,* **38,** L13502, doi:10.1029/2011GL047735.

Maykut, G. A., and M. G. McPhee, 1995: Solar heating of the Arctic mixed layer. *J. Geophys. Res.,* **100** (C12), 24 691–24 703.

McPhee, M. G., 1980: An analysis of pack ice drift in summer. *Sea Ice Processes and Models,* R. Pritchard, Ed., University of Washington Press, 62–75.

——, 2008: *Air–Ice–Ocean Interaction: Turbulent Ocean Boundary Layer Exchange Processes.* Springer, 215 pp.

——, 2012: Advances in understanding ice-ocean stress during and since AIDJEX. *Cold Reg. Sci. Technol.,* **76–77,** 24–36, doi:10.1016/j.coldregions.2011.05.001.

——, A. Proshutinsky, J. H. Morison, M. Steele, and M. B. Alkire, 2009: Rapid change in freshwater content of the Arctic Ocean. *Geophys. Res. Lett.,* **36,** L10602, doi:10.1029/2009GL037525.

Meier, W., F. Fetterer, K. Knowles, M. Savoie, and M. J. Brodzik, 2006: Sea ice concentrations from *Nimbus-7* SMMR and DMSP SSM/I-SSMIS passive microwave data. National Snow and Ice Data Center, Boulder, CO, digital media. [Available online at http://nsidc.org/data/docs/daac/nsidc0051_gsfc_seaice.gd.html.]

Morison, J., R. Kwok, C. Peralta-Ferriz, M. Alkire, I. Rigor, R. Andersen, and M. Steele, 2012: Changing Arctic Ocean freshwater pathways. *Nature,* **481,** 67–70, doi:10.1038/nature10705.

Nghiem, S. V., I. G. Rigor, D. K. Perovich, P. Clemente-Colon, J. W. Weatherly, and G. Neumann, 2007: Rapid reduction of Arctic perennial sea ice. *Geophys. Res. Lett.,* **34,** L19504, doi:10.1029/2007GL031138.

Ogi, M., and J. M. Wallace, 2012: The role of summer surface wind anomalies in the summer Arctic sea ice extent in 2010 and 2011. *Geophys. Res. Lett.,* **39,** L09704, doi:10.1029/2012GL051330.

——, I. G. Rigor, M. G. McPhee, and J. M. Wallace, 2008: Summer retreat of Arctic sea ice: Role of summer winds. *Geophys. Res. Lett.,* **35,** L24701, doi:10.1029/2008GL035672.

Persson, P. O. G., C. W. Fairall, E. L Andreas, P. S. Guest, and D. K. Perovich, 2002: Measurements near the Atmospheric Surface Flux Group tower at SHEBA: Near-surface conditions and surface energy budget. *J. Geophys. Res.,* **107,** 8045, doi:10.1029/2000JC000705.

Proshutinsky, A., R. H. Bourke, and F. A. McLaughlin, 2002: The role of the Beaufort Gyre in Arctic climate variability: Seasonal to decadal climate scales. *Geophys. Res. Lett.,* **29,** 2100, doi:10.1029/2002GL015847.

——, and Coauthors, 2009: Beaufort Gyre freshwater reservoir: State and variability from observations. *J. Geophys. Res.,* **114,** C00A10, doi:10.1029/2008JC005104.

Rabe, B., and Coauthors, 2011: An assessment of Arctic Ocean freshwater content changes from the 1990s to the 2006–2008 period. *Deep-Sea Res. I,* **58,** 173–185, doi:10.1016/j.dsr.2010.12.002.

Rigor, I. G., and J. M. Wallace, 2004: Variations in the age of Arctic sea-ice and summer sea-ice extent. *Geophys. Res. Lett.,* **31,** L09401, doi:10.1029/2004GL019492.

Saha, S., and Coauthors, 2010: The NCEP Climate Forecast System Reanalysis. *Bull. Amer. Meteor. Soc.,* **91,** 1015–1057.

Steele, M., R. Morley, and W. Ermold, 2001: PHC: A global ocean hydrography with a high-quality Arctic Ocean. *J. Climate,* **14,** 2079–2087.

——, W. Ermold, and J. Zhang, 2008: Arctic Ocean surface warming trends over the past 100 years. *Geophys. Res. Lett.,* **35,** L02614, doi:10.1029/2007GL031651.

Toole, J. M., R. A. Krishfield, M.-L. Timmermans, and A. Proshutinsky, 2011: The ice-tethered profiler: Argo of the Arctic. *Oceanography,* **24,** 126–135, doi:10.5670/oceanog.2011.64.

Yang, J., 2009: Seasonal and interannual variability of downwelling in the Beaufort Sea. *J. Geophys. Res.,* **114,** C00A14, doi:10.1029/2008JC005084.